Appl. Phys. A (2016) 122:905
DOI 10.1007/s00339-016-0448-2

Applied Physics A
Materials Science & Processing

Effect of substrate temperature on microstructure and electrical properties of $LaNiO_3$ films grown on SiO_2/Si substrates by pulsed laser deposition under a high oxygen pressure

Bin He[1] · Zhanjie Wang[1]

Received: 28 June 2016 / Accepted: 15 September 2016 / Published online: 21 September 2016

Abstract Lanthanum nickel oxide ($LaNiO_3$: LNO) thin films were deposited on SiO_2/Si(100) substrates by pulsed laser deposition under a high oxygen pressure of 50 Pa, and the effect of substrate temperature on the microstructure and electrical properties of the LNO films were studied by depositing the films at different temperatures. The results showed that the substrate temperature has a significant influence on the crystallinity, grain size, surface roughness and electrical resistivity of the LNO films, and the LNO films deposited at 650 °C show a low room-temperature resistivity of 420 μΩ cm. X-ray photoelectron spectroscopic analysis results revealed that the use of the high oxygen pressure in deposition process can avoid the oxygen loss in the films. The use of the LNO films as an electrode layer for the $BaTiO_3$ and $PbZr_{0.52}Ti_{0.48}O_3$ ferroelectric films was also confirmed, and the results indicate that the high-quality LNO films on Si substrates not only can be used as an electrode layer, but also as a seed layer to control the preferred orientation of ferroelectric films.

1 Introduction

Lanthanum nickel oxide ($LaNiO_3$: LNO) thin films have been extensively studied because they can be used as a bottom electrode in the fabrication of ferroelectric, piezoelectric and multiferroic devices. LNO is a perovskite-type metallic oxide with a pseudocubic lattice parameter of 0.384 nm, which matches well with that of most ferroelectric and multiferroic materials, such as Pb(Zr, Ti)O_3 [1, 2], (K, Na)NbO_3 [3], PMN-PT [4] and $BiFeO_3$ [5, 6], and the electrical resistivity at room temperature of epitaxial LNO thin films is the order of few hundred μΩ cm.

Since the initial works of Satyalakshmi et al. [7] and Prasad et al. [8], LNO films have been widely deposited by pulsed laser deposition (PLD) on several substrates such as $LaAlO_3$ [9–11], $SrTiO_3$ [9, 11–14] and Si [4, 15–18]. Usually, the epitaxial LNO films grown on single-crystal substrates of $LaAlO_3$ and $SrTiO_3$ show a low resistivity about 200–400 μΩ cm [10, 12, 13, 19], because these substrate materials have the same perovskite structure and their lattice constants are close to that of crystal LNO. However, these substrates are very expensive and cannot provide the geometry of the large size; in particular, they cannot be directly integrated with the Si-based circuit. On the other hand, the growth of LNO films on silicon substrate is still a challenge, because the obtained films are polycrystalline and their resistivity changes roughly from 1000 to 3700 μΩ cm [4, 15–17], which are even one order larger than those of epitaxial LNO films.

It is well known that LNO presents different resistivity values depending on the oxygen content. It has been reported that in bulk $LaNiO_{3-\delta}$, the resistivity changes from 790 to 5.35×10^3 μΩ cm for the oxygen stoichiometric δ varying from 0.02 to 0.14 [20]. The difference in δ occurs when the samples are subjected to different periods of time in an oxygen atmosphere. Sancheza et al. [17] reported that oxygen pressures during PLD process have a significant influence on the magnitude of the resistivity of LNO thin films and suggested that the high electrical resistivity of the films is caused by an oxygen deficiency. Jiang et al. [4] studied the effect of working pressure on resistivity of LNO films in the PLD process and reported

✉ Zhanjie Wang
wangzj@imr.ac.cn

[1] Shenyang National Laboratory for Materials Science, Institute of Metal Research, Chinese Academy of Sciences, 72 Wenhua Road, Shenyang 110016, China

that the resistivity linearly decreases with increasing working pressure up to 40 Pa and then increases oppositely. Recently, Awan et al. [18] fabricated LNO films on $SrTiO_3$-buffered Si(100) substrate by PLD and reported that the LNO films deposited at 600 °C under a oxygen pressure of 40 Pa show a low resistivity about 600 μΩ cm. The results mean that the growth of LNO films by PLD under a high oxygen pressure can avoid the oxygen loss in the films. On the other hand, the electrical resistivity of the LNO films is also sensitive to their microstructure, which can be controlled by deposition temperatures. For example, Sancheza et al. [17] deposited LNO films on CeO_2/YSZ-buffered Si(001) substrate at temperatures from 500 to 750 °C under a low oxygen pressure of 10 Pa and reported that the resistivity of the films changes from 4 to 12 mΩ cm. They surmised that the electrical properties of the films might be limited by local oxygen vacancies or by microstructure including microcracks and grain boundaries. However, the effect of substrate temperature on the microstructure and resistivity of LNO films deposited by PLD at a high oxygen pressure have not yet been studied systematically. In this study, in order to decrease the oxygen vacancy, LNO films are grown on SiO_2/Si(001) substrates by PLD at a high oxygen pressure of 50 Pa, and the effect of substrate temperature on microstructure and resistivity of the LNO films are investigated. The results show that the polycrystalline LNO films with a low resistivity of 420 μΩ cm can be obtained at 650 °C under the high oxygen pressure of 50 Pa, which is beneficial to fabricate high-quality ferroelectric films integrated with the Si-based circuit.

2 Experimental procedure

LNO thin films were grown on SiO_2/Si(001) substrates by PLD using a pulsed KrF excimer laser with a wavelength of 248 nm (Lambda Physik COMPexPro 201). The sintered ceramic disk of the LNO was used as a target for deposition. The LNO films were deposited under a high oxygen pressure of 50 Pa and at substrate temperatures of 575–725 °C for 10 min with a laser repetition rate of 2 Hz and laser fluence of 1 J/cm^2. The deposition rate of the LNO films was about 10 nm/min. The distance between the target and substrate was fixed at 4 cm. After deposition, high-purity oxygen was introduced into the growth chamber with working pressure up to 5×10^4 Pa, and the LNO films were annealed at the deposition temperature for 6 min and then cooled down to room temperature at a rate of 2 °C/min. To investigate the potential of the LNO films for use as a conductive/buffer layer for ferroelectric films, the ferroelectric $PbZr_{0.52}Ti_{0.48}O_3$ (PZT) and $BaTiO_3$ (BTO) thin films with a thickness of 200–300 nm were subsequently deposited on the LNO layers, respectively. The BTO or PZT films were deposited on the LNO film at a temperature of 650 °C for 20 min in the same run without vacuum breaking. Finally, these PZT/LNO and BTO/LNO bilayers were also cooled at a rate of 2 °C/min under oxygen pressure of 5×10^4 Pa.

The crystalline structure of the LNO films was examined by X-ray diffraction (XRD; Rigaku RINT2000, Tokyo, Japan, CuKα radiation) analysis. The surface morphology and roughness of the films were investigated using scanning electron microscopy (SEM: Supra 35; LEO, Oberkochen, Germany) and atom force microscope (AFM, Digital Instruments, Nanoscope IV). The cross-sectional microstructure of the films was studied by transmission electron microscopy (TEM, F20, Tecnai, Netherlands). Specimens for TEM were ground and polished to a thickness of 20 μm and were further thinned to perforation by Ar ion milling using a Gatan precision ion polishing system (PIPS, Gatan 691, Gatan Inc.; Pleasanton, CA). The resistivity of the LNO films was measured using a standard four-point probe method (MCP-T610, Tokyo, Japan). Chemical state of the elements in the films was determined by X-ray photoelectron spectroscopy (XPS, Therma ESCALAB 250; Al Kα source, 1486.60 eV), and all of the binding energies at different peaks were calibrated by using the C_{1s} photoelectron binging energy of 285.0 eV. The polarization versus electric field ($P - E$) hysteresis loops of the BTO and PZT ferroelectric films were measured by using a standard ferroelectric test system (TF2000E; Aixacct, Aachen, Germany).

3 Results and discussion

Figure 1a shows X-ray diffraction patterns of the LNO films deposited at different deposition temperatures from 575 to 725 °C. At the substrate temperature of 575 °C, the peaks of the perovskite phase weakly appear in the films. With increasing substrate temperature, the density of the diffraction peak of (110) planes gradually increases. The temperature dependence of FWHM value and grain size of the LNO films are shown in Fig. 1b. The FWHM values of the (110) diffraction peak monotonously decrease with increasing substrate temperature, indicating that the crystallinity of the films becomes well with increasing substrate temperature. On the other hand, the grain size calculated from the (110) diffraction peaks for the films evidently increases, indicating that the higher the substrate temperature, the more favorable the grain growth. This tendency has also been confirmed by AFM and SEM observations of the following. In addition, no secondary phase is detected in the films deposited at 650–725 °C, and the LNO films have a random orientation.

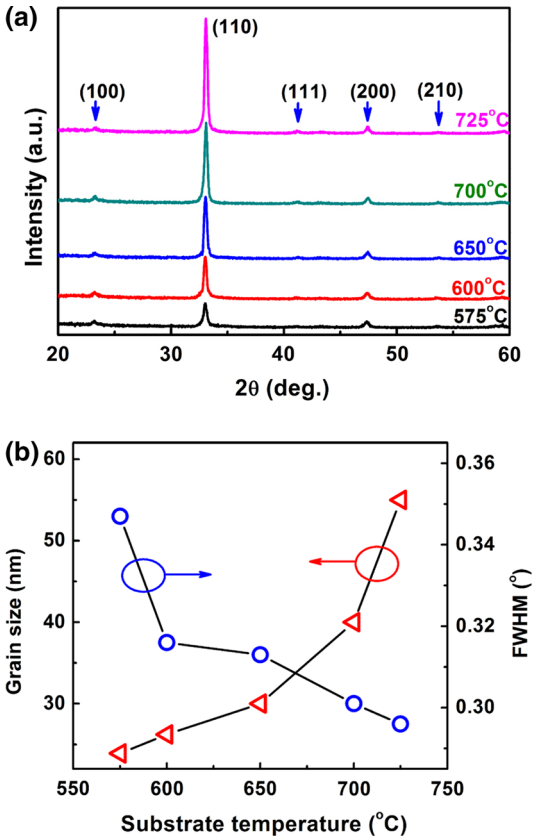

Fig. 1 **a** X-ray diffraction profiles of LNO thin films deposited at 575, 600, 650, 700 and 725 °C. **b** Temperature-dependent FWHM values and grain size for the LNO films

Figure 2a–e shows the AFM images of the LNO films deposited at various temperatures. It can be seen that the LNO films deposited at 575 °C show a featureless microstructure without the formation of visible grains on the surface, indicating that at such a low growth temperature, the deposited LNO films partly crystallized into the perovskite phase, which is consistent with XRD data (Fig. 1a). With increasing substrate temperature to 600 °C, grains can be clearly observed on the surface of the films. Further increasing the substrate temperature will lead to enlarged grain size and increased surface roughness. The tendency of grain size with substrate temperature is consistent with the XRD data (Fig. 1b). The substrate temperature dependence of root-mean-square (RMS) value of film surface roughness is displayed in Fig. 2f. For the given temperature region, the RMS value increases monotonously, because of the enlarged grain size. The differences in grain size and surface roughness between the films deposited at 600 and 725 °C have also been confirmed by SEM observation (Fig. 3). When deposited at 650 °C, the LNO films have fully crystallized and exhibited a smooth, uniform and dense microstructure and free of voids. In contrast, the grain size of the LNO films deposited at 725 °C is two times bigger than that of the LNO films deposited at 650 °C, and some voids can be observed at grain boundaries. The effect of the porosity on electrical resistivity of the LNO films will be discussed below.

Figure 4 shows the electrical resistivity of the LNO films as a function of deposition temperature. It can be seen that with increase in substrate temperature, the resistivity of the LNO films initially decreases rapidly and then increases oppositely. From 575 to 650 °C, the decrease in the resistivity of the LNO films is due to the better crystalline as shown by XRD data. On the other hand, the increase in the resistivity in the LNO films deposited over 650 °C can be explained on the basis of the results of the SEM and AFM observations. Although the crystallinity of the perovskite LNO films increases with increasing substrate temperature, numerous voids between grains are observed on the surface of the films deposited over 650 °C (Fig. 3b). Hence, it can be considered that the voids between grains increased the resistivity values of the LNO films [21]. The LNO films deposited at 650 °C exhibit the lowest resistivity, because they are mainly crystallized into the perovskite phase and their surface is very smooth, dense and void-free. The resistivity of the LNO films deposited at 650 °C is approximately 420 μΩ cm, which is much lower than that of LNO films deposited by PLD on Si substrates reported in Refs. [4, 15–18]. This is due to that the LNO films were deposited under the high oxygen pressure of 50 Pa, which may avoid the oxygen loss in the films. It is well known that the oxygen content has a significant influence on the magnitude of the resistivity of thin films and bulk $LNO_{3-\delta}$ [17, 20]. The oxygen deficiency in LNO deposition process will lead to change of nickel chemical valence state from +3 to +2, and the conductive properties deteriorate quickly due to the mixed existence of Ni^{2+} and Ni^{3+} [22, 23]. In order to understand the chemical valence state of the elements in LNO films deposited at 650 °C, X-ray photoelectron spectroscopy measurements were taken for the films. Figure 5a shows the high-resolution spectra from 885 to 830 eV, where the La 3*d* and Ni 2*p* peaks can be observed. Usually, the Ni $2p_{1/2}$ has a double peak for Ni^{2+}, but only a single peak for Ni^{3+} [10, 24]. As can be seen from Fig. 5a, the Ni $2p_{1/2}$ has a single peak, indicating that Ni ions occupy the Ni^{3+} state. It is clear that the change of Ni valence from Ni^{3+} to Ni^{2+} due to oxygen vacancies can be avoided by using the high oxygen pressure of 50 Pa in the film fabrication process.

On the other hand, the formation of oxygen vacancies can be directly observed by a decrease in lattice oxygen ratio in O 1*s* core-level photoelectron spectroscopy [25]. Figure 5b shows the high-resolution XPS spectra for O 1*s* of the films deposited at 650 °C. The O 1*s* peak can be deconvoluted into two peaks, and the major peak located at the lower binding energy (O 1*s*-*a*) is associated with lattice

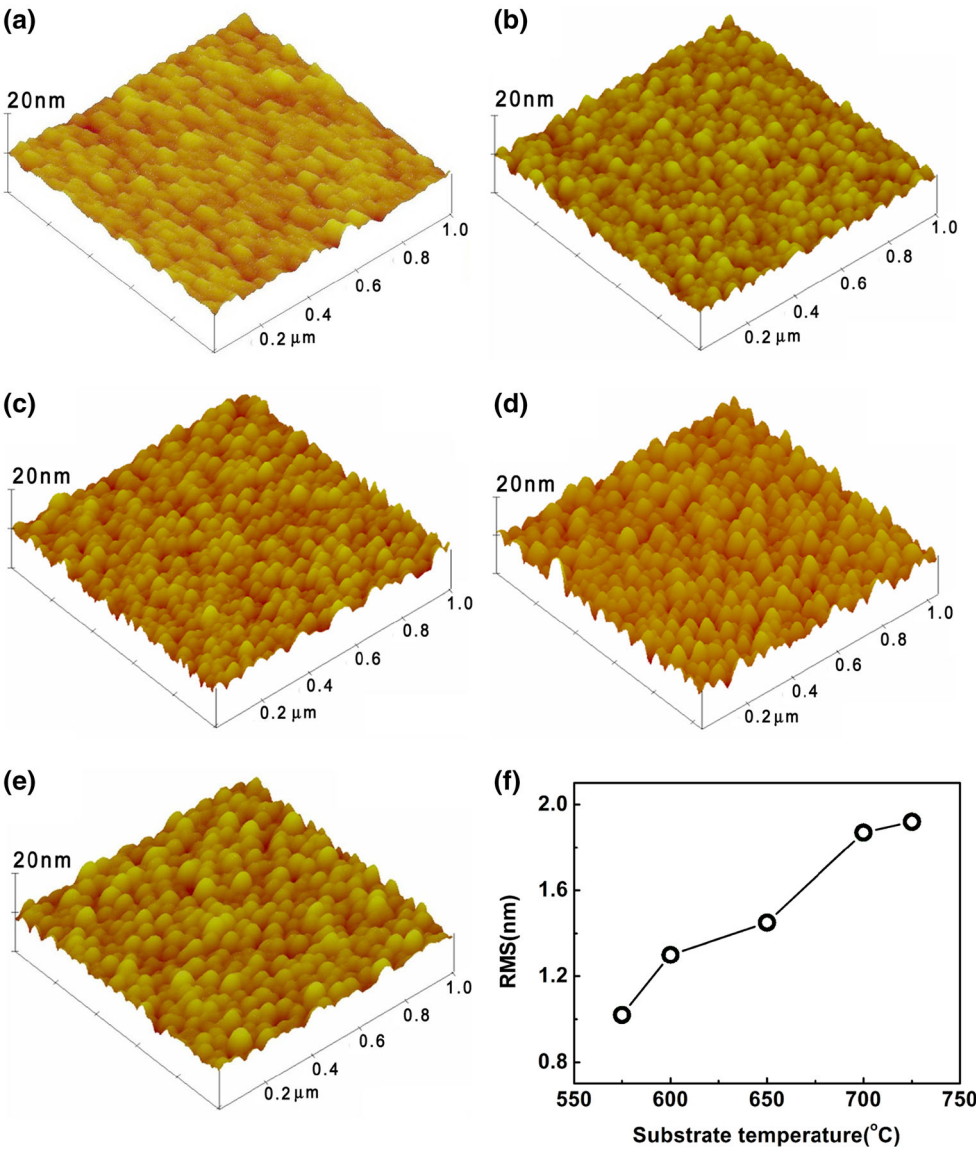

Fig. 2 AFM images of LNO films deposited at **a** 575 °C, **b** 600 °C, **c** 650 °C, **d** 700 °C, **e** 725 °C and **f** temperature-dependent RMS values for LNO films

oxygen in LNO, while the smaller peak located at the higher binding energy (O 1*s*-*b*) is associated with the surface absorptional oxygen [25, 26]. The relative intensity ratio (RIR) of O 1*s*-*a* to O 1*s*-*b* is approximately 3.29, which is much larger than that of the $LaNiO_3$ films deposited by radio frequency sputtering and post-annealed in oxygen pressure of 1 atm (approximately 2.18) [25]. The larger RIR also indicates no oxygen deficiency in the LNO film due to the high oxygen pressure of 50 Pa in the fabrication process.

To understand the conductive mechanism and transport property of the LNO films deposited at 650 °C, the temperature-dependent resistivity was further investigated, and the results are shown in Fig. 6. It can be seen that the resistivity of the LNO films monotonically decreases with decreasing temperature in the measured temperature range from 300 K down to 5 K, indicating a metallic transport mechanism in the films. There are two different behaviors in $\rho(T)$: For temperature above 40 K, the $\rho(T)$ is linear with T, and below 40 K, the $\rho(T)$ is quadratic with T. At low temperatures, the electrical resistivity curve is well fitted by the equation: $\rho(T) = a + cT^2$, where $a = 251.2$ μΩ cm; $c = 6.66 \times 10^{-3}$ μΩ cm/K^2 (shown in the lower inset of Fig. 6). Usually, the quadratic term in $\rho(T)$ has been related to electron–electron scattering. At high temperatures, the electrical resistivity curve is well fitted by the equation: $\rho(T) = a + bT$, where $a = 211.25$ μΩ cm, and $b = 0.792$ μΩ cm/K (shown in the upper inset of Fig. 6). The linear dependence is expected for a mechanism related to electron–phonon scattering. The same conductive mechanisms at low and high temperatures were reported in the high-quality LNO thin films grown on $SrTiO_3$ substrates [26, 27] and the bulk LNO [28]. Therefore, the above experimental results further confirmed that the

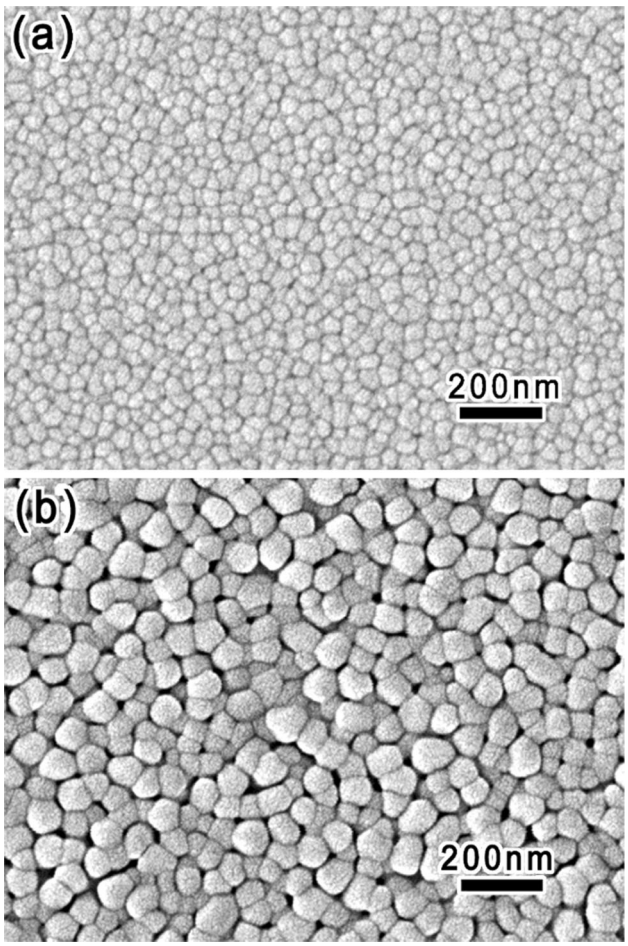

Fig. 3 Surface SEM images of LNO films deposited at **a** 650 °C and **b** 725 °C

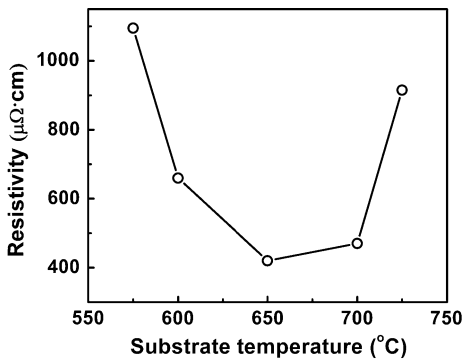

Fig. 4 Substrate temperature-dependent resistivity of LNO films

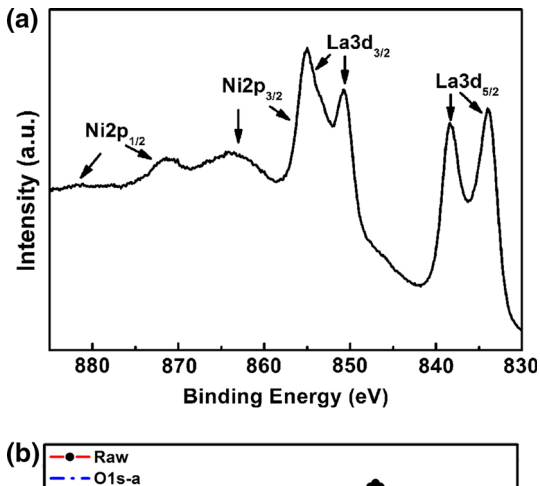

Fig. 5 **a** High-resolution XPS spectrum for Ni 2*p* and La 3*d* core-level lines of LNO films deposited at 650 °C. **b** High-resolution XPS spectrum for O 1*s* core-level line of LNO films deposited at 650 °C

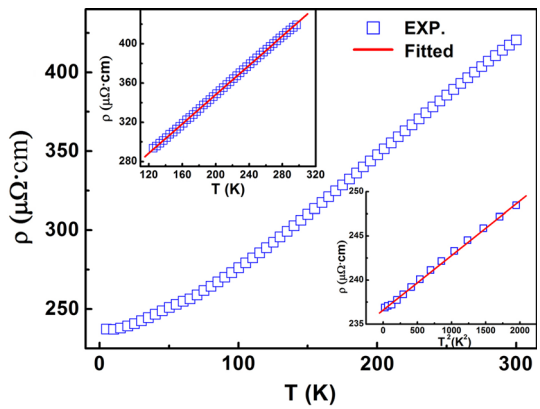

Fig. 6 Temperature-dependent resistivity of LNO films deposited at 650 °C

deposition under a high oxygen pressure in the PLD process can avoid oxygen loss in the LNO films. Moreover, by adjusting the deposition temperature to control the microstructure, the LNO films with good conductivity on silicon substrates can also be obtained, which are more suitable as a electrode layer for the fabrication of ferroelectric films.

To investigate its potential for use as a conductive/buffer layer for ferroelectric films, the BTO and PZT films were subsequently deposited on the LNO layer at a substrate temperature of 650 °C. Figure 7a is the XRD patterns of the BTO and PZT films, showing that the polycrystalline BTO and the PZT films have the perovskite phase, and no second phase can be detected in the films. In addition, the

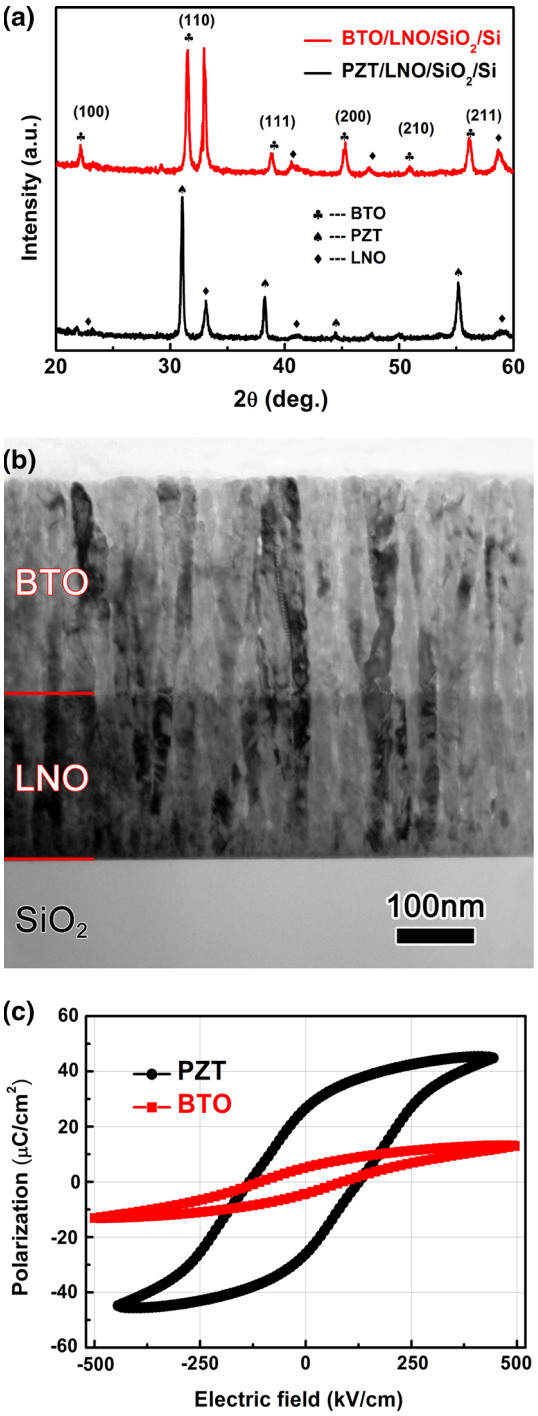

Fig. 7 **a** X-ray diffraction profiles of the BTO and PZT films on LNO/SiO_2/Si substrates. **b** A cross-sectional TEM image of the BTO film on the LNO/SiO_2/Si substrate. **c** $P - E$ hysteresis loops of the BTO and PZT films on LNO/SiO_2/Si substrates at room temperature

BTO and the PZT films have the (110)-preferred orientation, which is the same as the LNO film, indicating that the LNO film plays a role of the seed layer for the growth of the BTO and the PZT films. Figure 7b shows a cross-sectional TEM image of the BTO film on the LNO/SiO_2/Si substrate. It can be seen that the interface between the LNO and SiO_2 is very sharp and clear, but the interface between the BTO and LNO is not clear and can only be distinguished according to the difference of contrast between the two layers. The columnar perovskite grains of the BTO and LNO with the same contrast are continuous at the interface, indicating that the BTO perovskite grains were epitaxially grown on the surface of LNO perovskite grains. The ferroelectric properties of the BTO and PZT films were also investigated, and the results are shown in Fig. 7c. The BTO and PZT films exhibit a well-defined $P - E$ hysteresis shape. The remnant polarization (P_r) for the BTO and PZT films is about 4.8 and 26.1 μC/cm^2, which are comparable with those of the BTO and PZT films grown on the single-crystal substrates [29, 30]. The above results indicate that the high-quality LNO films not only can be used as an electrode layer, but also as a seed layer to control the preferred orientation of ferroelectric films.

4 Conclusion

In this study, polycrystalline LNO thin films have been deposited on SiO_2/Si(100) substrates by PLD under a high oxygen pressure of 50 Pa, and the effect of substrate temperature on the microstructure and electrical properties of the films were investigated. The structural, morphological and electrical properties of the films were characterized by XRD, FE-SEM, AFM, TEM and electrical resistivity. The chemical state of the elements in the films was determined by X-ray photoelectron spectroscopy. The analysis results revealed that substrate temperature has a considerable influence on the crystallinity, grain size, surface roughness and electrical resistivity of the LNO films. The use of the high oxygen pressure in deposition process can avoid the oxygen loss in the LNO films, and the LNO films deposited at 650 °C showed a low room-temperature resistivity of 420 μΩ cm. The BTO and PZT ferroelectric films deposited on the LNO layer had the (110)-preferred orientation and showed good ferroelectric properties, indicating that the high-quality LNO films not only can be used as an electrode layer, but also as a seed layer to control the preferred orientation of ferroelectric films.

Acknowledgments This work was supported by the Hundred Talents Program of the Chinese Academy of Sciences and the National Natural Science Foundation of China (No. 51172238).

References

1. H. Wang, Y. Bai, X. Ning, Z. Wang, RSC Adv. **5**, 104203 (2015)
2. Y.N. Chen, Z.J. Wang, J. Am. Ceram. Soc. **96**, 90 (2013)
3. T. Li, G. Wang, K. Li, N. Sama, D. Remiens, X. Dong, S. Trolier-McKinstry, J. Am. Ceram. Soc. **96**, 787 (2012)

4. J. Jiang, S.-G. Hur, S.-G. Yoon, J. Electrochem. Soc. **158**, G83 (2011)
5. F. Yan, T.J. Zhu, M.O. Lai, L. Lu, J. Appl. Phys. **110**, 084102 (2011)
6. J. Wu, J. Wang, J. Am. Ceram. Soc. **93**, 1422 (2010)
7. K.M. Satyalakshmi, R.M. Mallya, K.V. Ramanathan, X.D. Wu, B. Brainard, D.C. Gautier, N.Y. Vasanthacharya, M.S. Hegde, Appl. Phys. Lett. **62**, 1233 (1993)
8. K.V.R. Prasad, K.B.R. Varma, A.R. Raju, K.M. Satyalakshmi, R.M. Mallya, M.S. Hegde, Appl. Phys. Lett. **63**, 1898 (1993)
9. T. Yu, Y.F. Chen, Z.G. Liu, X.Y. Chen, L. Sun, N.B. Ming, L.J. Shi, Mater. Lett. **26**, 73–76 (1996)
10. K. Tsubouchi, I. Ohkubo, H. Kumigashira, Y. Matsumoto, T. Ohnishi, M. Lippmaa, H. Koinuma, M. Oshima, Appl. Phys. Lett. **92**, 262109 (2008)
11. M.K. Stewart, J. Liu, R.K. Smith, B.C. Chapler, C.H. Yee, R.E. Baumbach, M.B. Maple, K. Haule, J. Chakhalian, D.N. Basov, J. Appl. Phys. **110**, 033514 (2011)
12. F. Sanchez, C. Guerrero, M.V. Garcıa-Cuencaa, M. Varela, Appl. Phys. A **71**, 59 (2000)
13. B. Berini, W. Noun, Y. Dumont, E. Popova, N. Keller, J. Appl. Phys. **101**, 023529 (2007)
14. W. Noun, B. Berini, Y. Dumont, P.R. Dahoo, N. Keller, J. Appl. Phys. **102**, 063709 (2007)
15. L. Sun, T. Yu, T.F. Chen, J. Zhou, N.B. Ming, J. Mater. Res. **12**, 931 (1997)
16. J. Yin, X.Y. Chen, Q.C. Li, X.Y. Liu, Z.G. Liu, J. Mater. Res. **33**, 5631 (1998)
17. F. Sancheza, C. Ferratera, X. Alcobeb, J. Bassasb, M.V. Garcıa-Cuencaa, M. Varelaa, Thin Solid Films **384**, 200 (2001)
18. M.S. Awan, A.S. Bhatti, S. Qing, C.K. Ong, Vacuum **85**, 55 (2010)
19. M. Zhu, P. Komissinskiy, A. Radetinac, M. Vafaee, Z. Wang, L. Alff, Appl. Phys. Lett. **103**, 141902 (2013)
20. N. Gayathri, A.K. Raychaudhuri, X.Q. Xu, J.L. Peng, R.L. Greene, J. Phys. Condens. Matter **10**, 1323 (1998)
21. M.T. Escote, F.M. Pontes, E.R. Leite, J.A. Varela, R.F. Jardim, E. Longo, Thin Solid Films **445**, 54 (2003)
22. G. Wu, J.J. Neumeier, M.F. Hundley, Phys. Rev. B **63**, 245120 (2001)
23. B. Berini, N. Keller, Y. Dumont, E. Popova, W. Noun, M. Guyot, J. Vigneron, A. Etcheberry, N. Franco, R.M.C. da Silva, Phys. Rev. B **76**, 205417 (2007)
24. M. Medarde, A. Fontaine, J.L. García-Muñoz, J. Rodríguez-Carvajal, M. de Santis, M. Sacchi, G. Rossi, P. Lacorre, Phys. Rev. B **46**, 14975 (1992)
25. L. Qiao, X. Bi, Thin Solid Films **519**, 943 (2010)
26. C.R. Cho, D.A. Payne, S.L. Cho, Appl. Phys. Lett. **71**, 3013 (1997)
27. G.P. Mambrini, E.R. Leite, M.T. Escote, A.J. Chiquito, E. Longo, J.A. Varela, R.F. Jardim, J. Appl. Phys. **102**, 043708 (2007)
28. K. Sreedhar, J.M. Honig, M. Darwin, M. McElfresh, P.M. Shand, J. Xu, B.C. Crooker, J. Spalek, Phys. Rev. B **46**, 6382 (1992)
29. X.W. Wang, X. Wang, W.J. Gong, Y.Q. Zhang, Y.L. Zhu, Z.J. Wang, Z.D. Zhang, Thin Solid Films **520**, 2785 (2012)
30. D. Barrionuevo, N. Ortega, A. Kumar, R. Chatterjee, J.F. Scott, R.S. Katiyar, J. Appl. Phys. **114**, 234103 (2013)